Colloids and Surfaces B: Biointerfaces 107 (2013) 245–250

Contents lists available at SciVerse ScienceDirect

Colloids and Surfaces B: Biointerfaces

journal homepage: www.elsevier.com/locate/colsurfb

Hydrogen peroxide biosensor based on hemoglobin immobilized at graphene, flower-like zinc oxide, and gold nanoparticles nanocomposite modified glassy carbon electrode

Lingling Xie*, Yuandong Xu, Xiaoyu Cao*

School of Chemistry and Chemical Engineering, Henan University of Technology, Zhengzhou 450001, PR China

ARTICLE INFO

Article history:
Received 13 December 2012
Received in revised form 2 February 2013
Accepted 14 February 2013
Available online 24 February 2013

Keywords:
Flower-like zinc oxide
Au nanoparticles
Graphene
Hemoglobin
Biosensor

ABSTRACT

In this work, a highly sensitive hydrogen peroxide (H_2O_2) biosensor based on immobilization of hemoglobin (Hb) at Au nanoparticles (AuNPs)/flower-like zinc oxide/graphene (AuNPs/ZnO/Gr) composite modified glassy carbon electrode (GCE) was constructed, where ZnO and Au nanoparticles were modified through layer-by-layer onto Gr/GCE. Flower-like ZnO nanoparticles could be easily prepared by adding ethanol to the precursor solution having higher concentration of hydroxide ions. The Hb/AuNPs/ZnO/Gr composite film showed a pair of well-defined, quasi-reversible redox peaks with a formal potential (E^0) of −0.367 V, characteristic features of heme redox couple of Hb. The electron transfer rate constant (k_s) of immobilized Hb was 1.3 s^{-1}. The developed biosensor showed a very fast response (<2 s) toward H_2O_2 with good sensitivity, wide linear range, and low detection limit of 0.8 μM. The fabricated biosensor showed interesting features, including high selectivity, acceptable stability, good reproducibility, and repeatability along with excellent conductivity, facile electron mobility of Gr, and good biocompatibility of ZnO and AuNPs. The fabrication method of this biosensor was simple and effective for determination of H_2O_2 in real samples with quick response, good sensitivity, high selectivity, and acceptable recovery.

1. Introduction

Recently, there has been considerable interest in detection of H_2O_2 because of its wide and varied applications, such as the synthesis of various organic compounds, food production, clinical and pharmaceutical applications [1,2]. H_2O_2 is also used as an oxidant for liquid-based fuel cells [3,4] and has emerged as an important byproduct of enzymatic reactions in the field of biosensing [5,6]. So far, various methods have been used for H_2O_2 analysis, such as titrimetry [7], spectrophotometry [8], fluorometry [9], chemiluminescence [10], and chromatography [11]. Among the various methods, electrochemical methods have emerged as preferable, owing to their relatively low cost, simplicity, efficiency and high sensitivity [12,13]. Due to the high selectivity and specificity for H_2O_2, redox enzymes (horseradish peroxidase, cytochrome c, and hemoglobin [Hb])-based biosensors have been extensively employed for H_2O_2 detection [14–17]. Among these redox enzymes, Hb is an ideal model enzyme because of its known structure, commercial availability, and relatively higher stability [18]. Moreover, Hb has intrinsic peroxidaselike activity and could be an appropriate substitute for horseradish peroxidase, specifically for improving the biosensor performance and reducing the fabrication cost.

To enhance the performance features of the biosensor and to efficiently immobilize enzymes onto the electrode surfaces, various nanomaterial matrices have been used. Nano-sized ZnO is the most widely studied materials because of the stable chemical and physical character good biocompatibility, high surface activity, and rapid electron communication features [19,20]. AuNPs are a well-known kind of bionanomaterial because of their large specific surface area, strong adsorption ability, good suitability, and good conductivity [21,22]. AuNPs can strongly interact with biomaterials and have been utilized as an intermediator to immobilize antibody whilst efficiently retaining its activity and to enhance current response in the construction of a sensitive amperometric immunosensor. Therefore, AuNPs have been widely used in constructing electrical sensors such as DNA-AuNPs assemblies [23], enzymes biosensors [24], and immunosensors [25].

Graphene (Gr) has stimulated intense research interest because of its unique physical and chemical properties, such as high surface area, high electrical conductivity, good chemical stability, and strong mechanical strength [26–28]. Gr possesses many advantageous properties, such as the ease of material processing, low

* Corresponding author. Tel.: +86 371 67756718; fax: +86 371 67756718.
E-mail addresses: linglingxie@haut.edu.cn, linglingxie51@163.com (L. Xie), caoxy@haut.edu.cn (X. Cao).

0927-7765/$ – see front matter © 2013 Elsevier B.V. All rights reserved.
http://dx.doi.org/10.1016/j.colsurfb.2013.02.020

cost of synthesis, mechanical flexibility and ability to make composite materials. These merits make it an attractive candidate for fabricating various functional devices, such as electrodes [29], sensors [30], photovoltaics [31] and photodetectors [32]. Moreover, two-dimensional plane structure of Gr provides a vast platform for loading various nanoparticles, offering a new way to develop catalytic, magnetic, and optoelectronic materials [33]. It has also been reported that the integration of carbon-based materials and metal nanoparticles or metal oxide usually shows synergistic effects in electrocatalytic applications [34], so there is a reason to expect the integration of Gr, nano-sized ZnO and AuNPs has the similar effect.

Due to the good biocompatibility and conductivity of Gr, nano-sized ZnO and AuNPs, they were chosen to modify the GCE for the retention of Hb's biological activity and improvement of the electron transfer between Hb and electrodes. The biosensor based on Hb/AuNPs/ZnO/Gr composite film was fabricated to improve their electroactivity for H_2O_2. Electrochemical behavior of the sensor was studied in detail. Direct electron transfer between Hb and GCE and the electrocatalytic reduction of H_2O_2 at the biosensor were observed.

2. Experimental

2.1. Chemicals and materials

Graphite powder, hydrazine solution (50 wt%) and ammonia solution (28 wt%) were purchased from Shanghai Chemical Reagent Corporation (Shanghai, China). Chloroauric acid and 3-Aminopropyl triethylene silane (APS) was obtained from Shuguang Chemical Co. (Nanjing, China). Phosphate buffer solution (PBS) was prepared by mixing stock standard solution of Na_2HPO_4 and NaH_2PO_4. Hb was obtained from Sigma (St. Louis, MO, USA). All chemicals were of analytical grade and doubly distilled water was used throughout.

2.2. Apparatus

Electrochemical measurements were performed on a CHI 660C Electrochemical Workstation (Shanghai CH Instruments, China). A conventional three-electrode system was used throughout the experiments. The working electrode was a bare, a pretreated or Hb/AuNPs/ZnO/Gr composite modified GCE (3.0 mm in diameter); the auxiliary electrode was a platinum wire and a saturated calomel electrode (SCE) was used as the reference. Electrochemical impedance spectroscopy (EIS) was performed in 5.0 mM $K_3Fe(CN)_6/K_4Fe(CN)_6$ (1/1) mixture with 0.1 M KCl as supporting electrolyte, using an alternating current voltage of 5 mV, within the frequency range of 0.1–10^5 Hz by Autolab Electrochemistry Instruments (Autolab, Eco Chemie, The Netherlands). The morphologies of the nanocomposite were recorded on a Hitachi S-4800 scanning electron microscope (SEM).

2.3. Preparation of graphene and its functionalized products

Graphene oxide (GO) was prepared from graphite powder by the Hummers method [35]. To get Gr, chemical reduction of the suspension of GO was carried out with hydrazine monohydrate for 24 h at 80 °C. The final product was isolated by filtration, and rinsed thoroughly with pure water and ethanol. Then the product was dried in vacuum and Gr was obtained.

2.4. Preparation of gold nanoparticles

Au nanoparticles were prepared by a method previously reported [25] with a slight modification. 200 mL of water and 2 mL of 1% (w/w) $HAuCl_4$ solution were mixed and heated to boiling with continuous stirring. Then 4.0 mL of a 1% (w/w) sodium citrate solution was quickly added. The solution turned purple within 20 s and then wine-red color 60 s later. After 15 min, the heater was removed and the mixture was stirred continuously until cooled. Colloidal Au solution was obtained and stored in a dark glass bottle at 4 °C before use.

2.5. Preparation of nano-sized ZnO

Ina typical procedure to synthesize flower-like ZnO nanostructures, 0.2 g of $Zn(NO_3)\cdot 6H_2O$ was dissolved in 15 mL of water and to this 0.8 g of NaOH in 10 mL of water was added slowly under constant stirring. After stirring for 5 min at room temperature, 100 mL of ethanol was added slowly and stirred for further 5 min. The final white precipitate was separated by centrifugation, and washed with water and ethanol several times and dried in vacuum.

2.6. Preparation of Hb/AuNPs/ZnO/Gr modified GCE

The electrode preparation was according to the following steps. The GC electrode was polished with 1.0, 0.3, and 0.05 μm Al_2O_3 powder in sequence, and then rinsed thoroughly with deionized water and sonicated in deionized water and ethanol, respectively. 1.0 mg Gr was dispersed in 1.0 mL N,N-dimethylformamide and the as-prepared dispersion was sonicated for 30 min to form a homogeneous black suspension and then an 8 μL drop of solution was placed on a 3 mm diameter of GCE, and allowed to dry under ambient condition to obtain Gr/GCE. 1.0 mg ZnO was dispersed in 1.0 mL APS solution (2%, v/v) and sonicated for 20 min to form a homogeneous suspension and then a 8 μL drop of solution was placed on Gr/GCE, and allowed to dry under ambient condition to obtain ZnO/Gr/GCE. Then, the electrode was rinsed thoroughly with water and dipped into AuNPs solution for 12 h, then rinsed with water to obtain AuNPs/ZnO/Gr/GCE. Subsequently, 10.0 μL of 5.0 mg mL^{-1} Hb solution in PBS (pH 7.0) were dropped onto the GCE surface and dried in room temperature. So that the Hb/AuNPs/ZnO/Gr modified electrode was obtained. When not in use, the electrodes were stored at 4 °C in a refrigerator.

3. Results and discussion

3.1. Characterization

The morphology of the as-prepared nanocomposite was examined by SEM. Fig. 1a showed the SEM image of the obtained Gr sheet, illustrating the flake-like shapes of Gr. A low-magnification view of the as-prepared ZnO nanostructures (Fig. 1b) shows the high yield and uniformity of the synthesized products. The magnified SEM image in Fig. 1c shows that the morphology of ZnO product is well-defined flower-like structure. The diameter of the flowers are around 4 μm, assembled by many nano sheets as "petals". Fig. 1d depicts the structure of the surface of AuNPs/ZnO/Gr composite film. As shown in this image, AuNPs were embedded in the surface of ZnO-APS/Gr composite. It can be seen that the AuNPs were exhibiting a homogeneous distribution on the electrode surface.

FT-IR spectroscopy, which could provide some useful information on the structure and conformation of protein molecules, were also employed to investigate the existing state of the immobilized Hb. The shapes of amide I (1700–1600 cm^{-1}) and amide II (1600–1500 cm^{-1}) infrared absorption bands of proteins provide detailed information on the secondary structure of the polypeptide chain [36]. Curve a in Fig. 2 (A) shows the spectrum of native Hb, with amide I band at 1650 cm^{-1} caused by the C=O stretching vibrations of the peptide linkage and amide II band at 1545 cm^{-1} resulted from a combination of N—H in-plane bending and C—N stretching of the peptide groups, respectively. The spectrum of

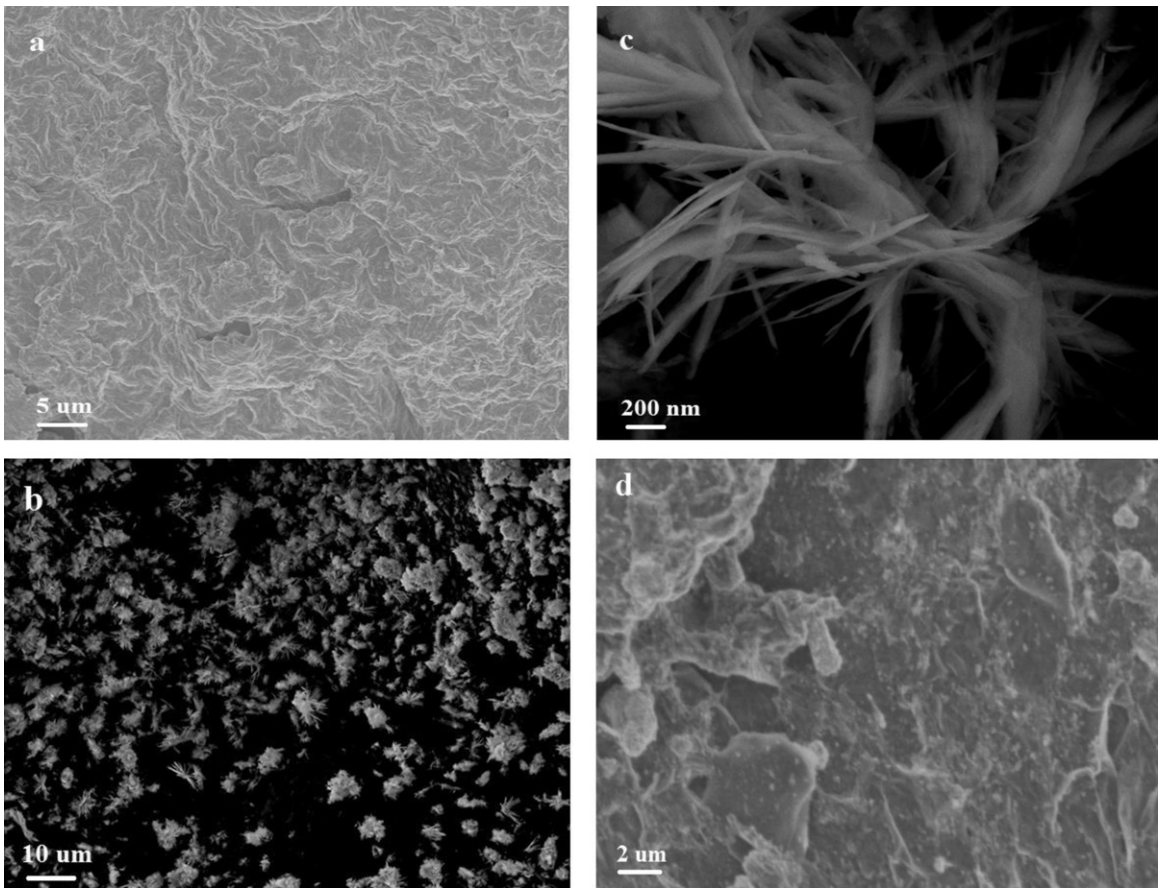

Fig. 1. SEM images of Gr (a), ZnO (b), high-magnification view of b (c), and AuNPs/ZnO/Gr (d).

Hb/AuNPs/ZnO/Gr composite film displays the combination shape of those of its components (curve b). While, the positions of the both amide bands for the compostie film are similar to those of the pure Hb. The present data support the speculation that the major portion of Hb essentially retains its native structure in the composite film.

UV–vis spectroscopy is an effective tool for monitoring the possible change of the Soret absorption band in the heme group region. The band shift may provide the information of possible denaturation of heme protein, especially that conformational change around the heme region [36]. Fig. 2(B) shows the UV–vis spectra of pure Hb (curve a) and Hb/AuNPs/ZnO/Gr composite (curve b), respectively. For the entrapped Hb with AuNPs/ZnO/Gr composite, the Soret band showed the peak location at 414 nm, shifting only 2 nm toward the red in comparison with that of the pure Hb. The slight shift in Soret band and the decrease in its absorbance may be due to the interaction between the composite film and proteins. Such interactions neither destroy the structure nor change the fundamental microenvironment of the biomolecules. One point should be highlighted that there is an absorption peak at about 535 nm on the AuNPs/ZnO/Gr composite film which does not appear on the spectrum of pure Hb and which is ascribed to the characteristic absorption peak of Au nanoparticles.

3.2. Direct electron transfer reactivity of the Hb/AuNPs/ZnO/Gr/GCE

Fig. 3(B) shows the cyclic voltammograms (CVs) of different electrodes in 0.1 M phosphate buffer solution, pH 7.0 (PBS) at a scan rate of 100 mV s^{-1}. The Hb on GCE showed no electrochemical redox peak in the potential range studied (curve a). It is well known that the heme prosthetic group of Hb is deeply embedded in a protective protein shell, which makes the direct electron communication with electrodes extremely difficult. The Hb/Gr/GCE (curve b) shows a couple of very small and broad redox peaks. The background current of Hb/Gr/GCE is very large because of the good conductivity of Gr. As to the Hb/ZnO/Gr/GCE, two well defined redox peaks are found in curve c, because nano-sized ZnO has good biocompatibility, high surface activity, and rapid electron communication features. AuNPs is a kind of well known bio-nanomaterials because of their large specific surface area, strong adsorption ability, well suitability and good conductivity. It can strongly interact with biomaterials and has been utilized as an intermediator to immobilize biomolecule to efficiently retain its activity and to enhance current response in the construction of an electrochemical biosensor. As indicated by curve d, immobilization of Hb on the AuNPs/ZnO/Gr/GCE shows a pair of well-defined and nearly symmetric redox anodic and cathodic peaks. Shapes of anodic to cathodic peaks are nearly symmetric, and the heights of reduction and oxidation peaks are the same. Obviously, the response of the Hb/AuNPs/ZnO/Gr/GCE is attributed to the redox of the electroactive center of Hb on the electrode surface. The results suggest that the Hb molecules entrapped in the composite film retained the electrochemical activity.

The improvement of the film conductivity in the present of AuNPs/ZnO/Gr composite film can be supported by AC impedance studies. Fig. 3(B) exhibits the electrochemical impedance spectra of the electrode surface status. The electron transfer resistance (R_{et}) at the electrode surface is equal to the semicircle diameter, which can be used to describe the interface properties of the electrode. Curve a in Fig. 3(B) shows the electrochemical impedance spectrum of the bare GCE. The semicircle domain of it is small (R_{et} = 650 Ω), implying a very low electron transfer resistance to the

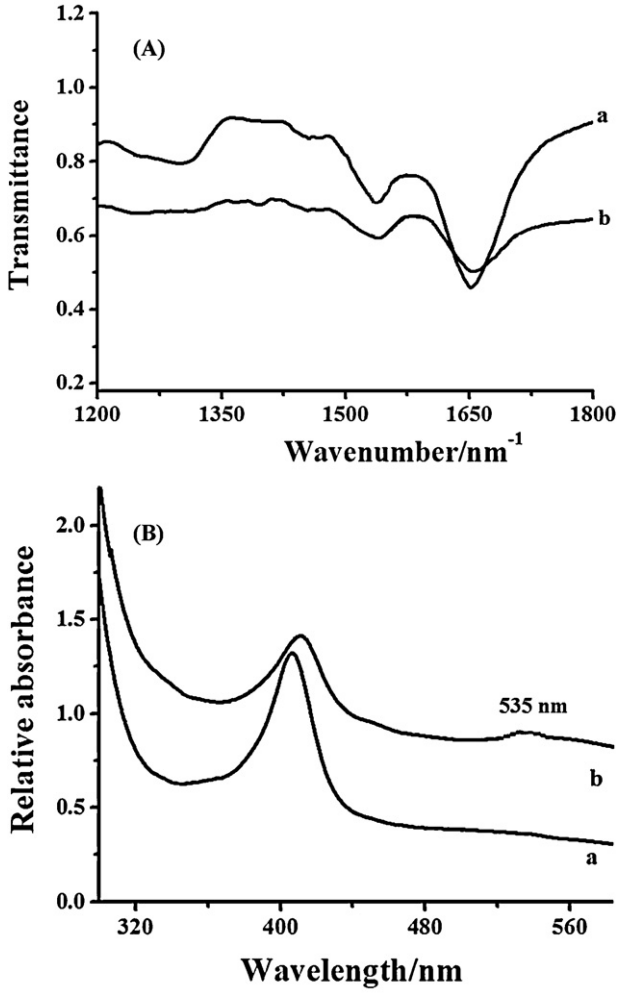

Fig. 2. (A) FT-IR spectra of pure Hb (a), and Hb/AuNPs/ZnO/Gr composite (b). (B) UV–vis absorption spectra of pure Hb (a), and Hb/AuNPs/ZnO/Gr (b).

redox-probe dissolved in the electrolyte solution. It was observed that the electrochemical impedance spectroscopy of Gr/GCE (curve b) and ZnO/Gr/GCE (curve c) display an almost straight line in the Nyquist plot of impedance spectroscopy, characteristics of a diffusion-limited electron-transfer process. This indicated that the conductivity of the Gr and nano-sized ZnO were essentially beneficial to the electron transfer. The AuNPs/ZnO/Gr/GCE film increases the R_{et} to about 200 Ω (curve d), indicating the successful introduction of AuNPs into the ZnO/Gr composite film. When Hb immobilized onto AuNPs/ZnO/Gr/GCE (curve e), the resistance for the modified electrode increases greatly (1500 Ω). This is caused by the nonconductive property of Hb which acts as an inert electron layer and retarded the electron transfer.

Further study shows that the electrode potential of the redox peak strongly depends on the pH of the electrolytes (Fig. 4(A)). The effect of pH on the electrochemical behavior of Hb in AuNPs/ZnO/Gr/GCE film had been examined by CV. Increasing with the pH of the PBS, both the cathodic and anodic peak of Hb showed a negative shift. In the pH range from 5.0 to 9.0, the apparent standard potential (E^0) showed a linear dependence on the pH value of buffer with a linear regression equation as E^0 (V) = −0.049pH − 0.067 (R = 0.9954) (Fig. 4(A)). The slope value of the plot is −49 mV pH^{-1}, which is reasonably close to the theoretical value of −59 mV pH^{-1} at 291.15 K for a reversible one-proton coupled to a single electron transfer. This further supports the response of the Hb/AuNPs/ZnO/Gr/GCE biosensor being due to the redox reaction of the immobilized on the electrode surface. In order to provide a favorable microenvironment for Hb, pH 7.0 was chosen.

Fig. 4(B) shows the CVs of Hb/AuNPs/ZnO/Gr/GCE with different scan rates in pH 7.0 PBS. A pair of roughly symmetric redox peaks appeared with almost equal heights of the redox peak currents in the scan rate from 20 to 200 mV s^{-1}. The results indicate that all the electroactive Hb Fe(III) in the film were reduced to Hb Fe(II) on the forward scan and then reoxidized to Hb Fe(III) on the reverse scan. A good linear relationship was found (inset of Fig. 4(B)) between the redox peak current and scan rate with the results as I_{pc} (μA) = 5.460 + 0.7631ν (mV s^{-1}) (R = 0.9972) and I_{pa} (μA) = −1.772 − 0.3186ν (mV s^{-1}) (R = 0.9912). This revealed that the electron transfer between Hb and GCE is a surface-controlled electrochemical process and the immobilized Hb on AuNPs/ZnO/Gr film is not denatured. Based on the integration of the cyclic voltammetric reduction peaks and Faraday's laws, the surface concentration of the electroactive substance (Γ_c) is estimated according to the following formula [37]:

$$Q = nFA\Gamma_c \quad (1)$$

where Q is total amount of charge passed through the electrode for the reduction reaction, n is the number of electron transferred, F is the Faraday's constant, and A is the geometric area of GCE. The charge values (Q) are nearly constant in different scan rates, which range from 20 to 200 mV s^{-1}. The average value of Γ_c is calculated as 6.7×10^{-9} mol cm^{-2}, while the theoretic value of surface concentration is 8.8×10^{-9} mol cm^{-2}, which is calculated by the absolute concentration of Hb on the geometric area of GCE. This illustrates that approximately 77.3% of the total amount of Hb in the film play a part in the electron transfer progress. The theoretical monolayer coverage of Hb on the electrode surface was approximately 1.89×10^{-11} mol cm^{-2} [38,39], so it can be concluded that several layers of Hb immobilized on the electrode surface participate in the electrochemical reaction. The results indicate that the AuNPs/ZnO/Gr film with a large surface area and high loading content of Hb contributed to the multi-layer of protein participating in the electron transfer process.

The peak-to-peak separation (ΔE_p) increased gradually with the increase of scan rate, indicating that the electrode process is quasi-reversible. As $\Delta E_p \leq 200$ mV, the electron transfer rate constant (K_s) of Hb on the modified electrode is estimated to be 1.3 s^{-1} which is in the range of surface-controlled quasi-reversible redox process

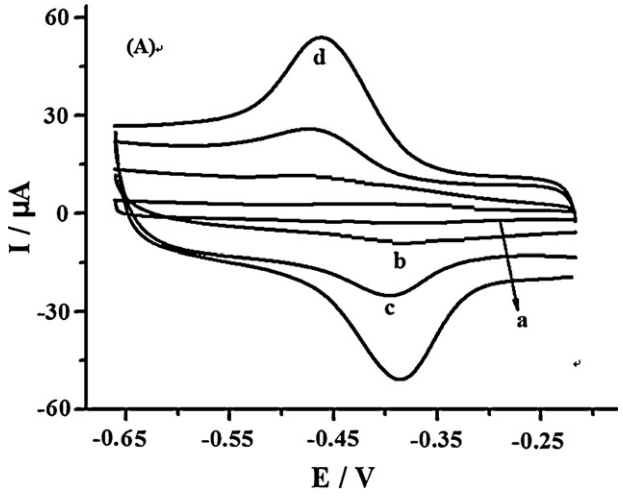

Fig. 3. (A) CVs of Hb/GCE (a), Hb/Gr/GCE (b), Hb/ZnO/Gr/GCE (c), and Hb/AuNPs/ZnO/Gr/GCE (d) in 0.1 M pH 7.0 PBS. Scan rate: 50 mV s^{-1}. (B) Nyquist plots at bare GCE (a), Gr/GCE (b), ZnO/Gr/GCE (c), AuNPs/ZnO/Gr/GCE (d) and Hb/AuNPs/ZnO/Gr/GCE (e) in 5 mM $Fe(CN)_6^{3-/4-}$ containing 0.1 M KCl. The frequency range is from 0.1 Hz to 10 kHz.

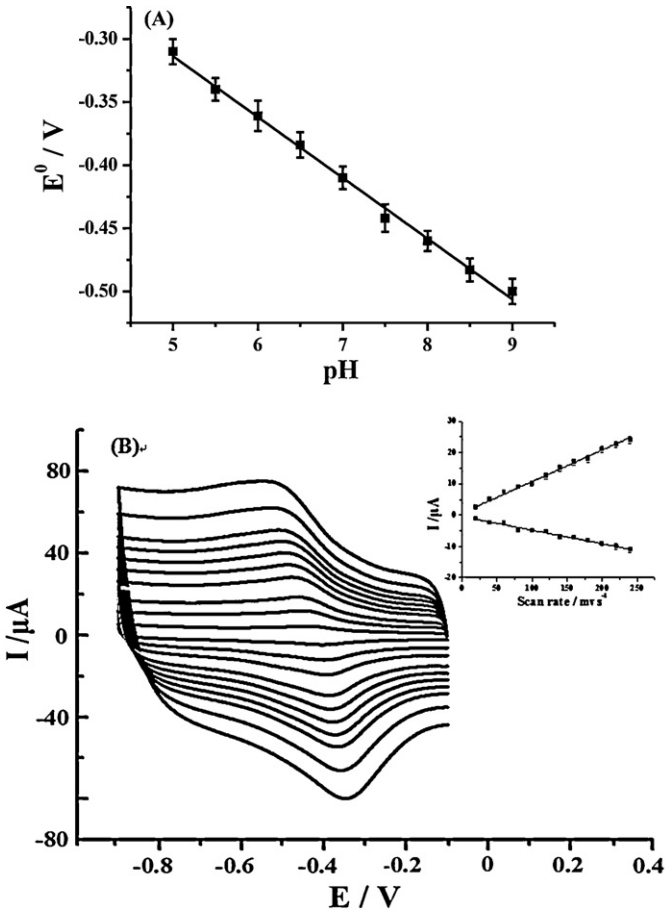

Fig. 4. (A) Plots of peak potential vs. pH. (B) CVs of Hb/AuNPs/ZnO/Gr/GCE in 0.1 M PBS (pH 7.0) at different scan rates. Scan rate (inside to outside): 20, 40, 60, 80, 100, 120, 140, 160, 180, 200 mV s^{-1}. Inset: plots of peak current vs. scan rates (error bars show SD of three measurements).

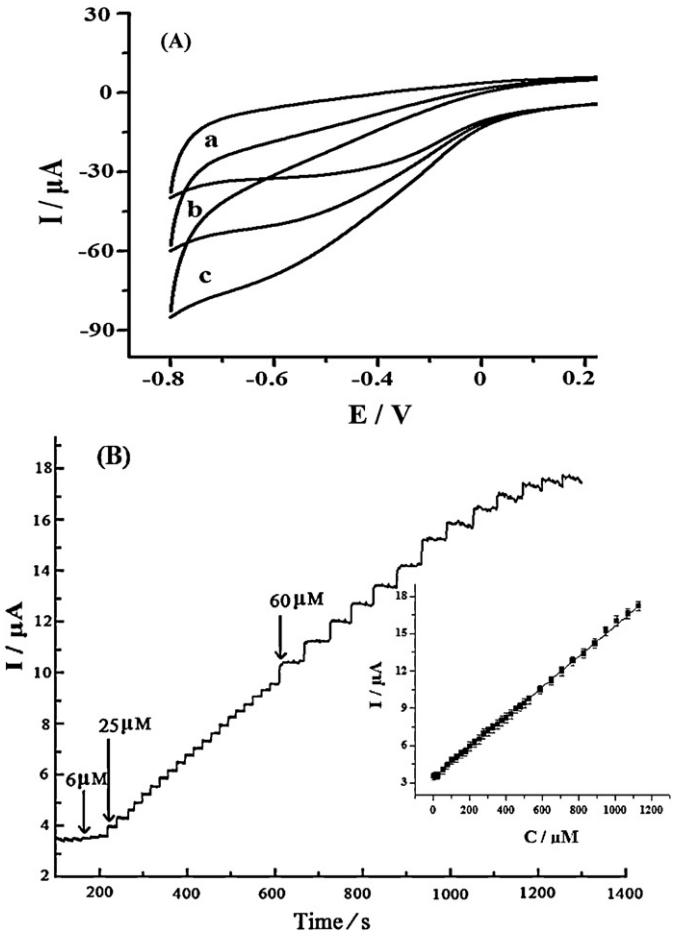

Fig. 5. (A) CVs of Hb/AuNPs/ZnO/Gr/GCE in the absence (a) and presence of 3.0×10^{-4} mol L^{-1} (b), 6.0×10^{-4} mol L^{-1} (c) H_2O_2 in 0.1 M PBS (pH 7.0). Scan rate: 100 mV s^{-1}. (B) Amperometric response of Hb/AuNPs/ZnO/Gr/GCE to successive addition of 6 μM, 25 μM and 60 μM H_2O_2 (inset: the plot of current versus H_2O_2 concentration) (error bars show SD of three measurements).

of Hb [40], and is larger than those obtained for Hb–TiO_2 whisker film modified GCE (0.59 s^{-1}) [41], and Hb immobilized on azide-terminated organic self-assembled monolayers (SAMs) modified Au electrode (0.78 s^{-1}) [42], etc. Such results revealed a reasonably fast electron transfer between the immobilized Hb and the underlying electrode.

3.3. Electrochemical catalysis of H_2O_2

To explore the potential application of Hb/AuNPs/ZnO/Gr/GCE, the electrocatalytic reduction of different amount of H_2O_2 on the electrode has been studied by CVs. When H_2O_2 was added into a pH 7.0 PBS, a dramatically increase of the cathodic peak current was observed (Fig. 5(A)). However, no similar cathodic peak corresponding to the reduction of H_2O_2 could be observed at GCE and AuNPs/ZnO/Gr/GCE under the same condition, so it could be concluded that Hb/AuNPs/ZnO/Gr/GCE showed good catalytic activity toward H_2O_2. Also, this obvious increase in the cathodic current indicated that the Hb kept its natural structure after immobilizing in the AuNPs/ZnO/Gr composite film modified GCE.

The amperometric response to H_2O_2 at the modified electrode was investigated by successively adding H_2O_2 to a continuous stirring PBS solution. Fig. 5(B) shows the steady-state amperometric response of the biosensor to the successive addition of aliquot H_2O_2 into the PBS with an operating potential of −300 mV. The inset shows a calibration plot based on reduction current responses in the presence of H_2O_2. The sensor could achieve more than 98% of the steady-state current within 2 s, indicating a fast amperometric response to H_2O_2 reduction. The current response toward H_2O_2 concentration was linear from 6.0 to 1130 μM. The detection limit was estimated to be 0.8 μM (S/N = 3). The relative standard deviation of the biosensor response to 10 μM H_2O_2 was 3.1% for three successive measurements.

A comparison of electroanalytical values of various modified electrodes for H_2O_2 detection using different techniques was listed in Table 1. The comparative data suggested superiority of the present sensor over some earlier reported methods, especially the detection limit and linear range.

When the concentration of H_2O_2 was further added, a response plateau showing the characteristics of the Michaelis-Menten kinetic mechanism was observed. The apparent Michaelis-Menten constant (K_M), which gives an indication of the enzyme-substrate kinetics, can be obtained from the Lineweaver-Burk equation:

$$\frac{1}{I_{ss}} = \frac{1}{I_{max}} + \frac{K_M}{I_{max}} \cdot \frac{1}{C}$$

where I_{ss} is the steady-state current after the addition of substrate, which can be obtained from amperometric experiments, I_{max} is the maximum current measured under saturated substrate solution and C is the bulk concentration of the substrate. The value of the apparent Michaelis-Menten constant (K_M) can be calculated from the slope ($K_M/I_{max} \cdot 1/C$) and the intercept ($1/I_{max}$) for the plot of the reciprocals of the steady-state current (I_{SS}) versus H_2O_2

Table 1
The performances of the various types of modified electrodes.

Modified electrode	Linear range (μM)	LOD (μM)	Stability[a] (percentage/days)	Reference
HRP in nano-Au/carbon ceramic electrode	12.2–1100	6.1	75%/35	[43]
Hb in nano-Au/ITO	10–7000	4.5	75%/40	[44]
Hb in eggphosphatidylcholine/pyrolytic graphite electrode	10–100	3.90	90%/14	[45]
Hb in silica sol–gel/carbon paste electrode	1–280	0.86	93%/21	[46]
Hb in carbon nanotube powder microelectrodes electrodes	210–900	9.00	Not reported	[47]
Hb in thiolated-viologen/Au electrode	10–125	0.25	90%/30	[48]
Hb in CHT/nano-$CaCO_3$/GCE	37–830	8.30	Not reported	[49]
Hb in chit/AuNPS/APS/PB/GCE	2–480	0.10	93%/20	[36]
Hb in AuNPS/ZnO/Gr/GCE	6.0–1130	0.8	94.2%/21	This work

[a] The biosensor retained percentage of its initial response after a storage period.

concentration (C). K_M can be obtained by the analysis of slope and intercept of the plot of the reciprocals of the steadystate current versus H_2O_2 concentration. The K_M value of Hb/AuNPs/ZnO/Gr/GCE was estimated to be 0.17 mM. As is well known the smaller K_M shows the higher catalytic ability. The low value of K_M indicated that the modified electrode exhibited a high affinity for H_2O_2 and prepared a sufficient microenvironment for enzyme-substrate interaction.

3.4. Repeatability and stability of the Hb/AuNPs/ZnO/Gr/GCE

The storage stability of Hb/PNNS/MWCNTs/GCE was studied by storing the electrode at 4 °C for about 3 weeks, and the sensor retained 94.2% of its original response to H_2O_2. Reproducibility of the biosensor system was evaluated from the response for 10 μM H_2O_2 at six electrodes and the relative standard deviation (RSD) value of 2.54% was observed. The good long-term stability can be attributed to the good biocompatibility of the nanocomposite film, which can provide a favorable microenvironment for Hb to retain its bioactivity.

4. Conclusions

A novel amperometric H_2O_2 biosensor was proposed based on the Hb immobilized on an AuNPs/ZnO/Gr/GCE. The nano-sized ZnO nanoparticles possess good biocompatibility and conductivity. The ZnO-APS-AuNPs composite has good uniformity and are ready for protein immobilization. Gr have large specific surface area, and can improve the conductivity and mechanical properties of the ZnO-APS-AuNPs composite. Combining the advantages of nano-sized ZnO, AuNPs and Gr, the Hb/AuNPs/ZnO/Gr/GCE biosensors show good analytical performance, such as high sensitivity, acceptable fabrication reproducibility, and storage stability. The present investigation demonstrates that the AuNPs/ZnO/Gr/GCE can provide an elegant platform for the study on the direct electrochemistry of redox enzymes and the construction of amperometric third-generation biosensors. In addition, it provides a promising application for nanoparticles materials for the study of direct electron transfer of proteins and the development of biosensors.

References

[1] A. Salimi, R. Hallaj, S. Soltanian, H. Mamkhezri, Anal. Chim. Acta 594 (2007) 24–31.
[2] Y. Usui, K. Sato, M. Tanka, Angew. Chem. Int. Ed. 42 (2003) 5623–5625.
[3] N.A. Choudhury, R.K. Raman, S. Sampath, A.K. Shukla, J. Power Sources 143 (2005) 1–8.
[4] S. Hasegawa, K. Shimotani, K. Kishi, H. Watanabe, Electrochem. Solid State Lett. 8 (2005) A119–A121.
[5] M.D. Gouda, M.A. Kumar, M.S. Thacur, N.G. Karanth, Biosens. Bioelectron. 17 (2002) 503–507.
[6] D. Shan, M.J. Zhu, H.G. Xue, S. Cosnier, Biosens. Bioelectron. 22 (2007) 1612–1617.
[7] N.V. Klassen, D. Marchington, H.C.E. Mcgowan, Anal. Chem. 66 (1994) 2921–2925.
[8] P.A. Tanner, A.Y.S. Wong, Anal. Chim. Acta 370 (1998) 279–287.
[9] I. Mori, K. Takasaki, Y. Fujita, T. Matsuo, Talanta 47 (1998) 631–637.
[10] A.N. Diaz, M.C.R. Peinado, M.C.T. Minguez, Anal. Chim. Acta 363 (1998) 221–227.
[11] J.G. Hong, J. Maguhn, D. Freitag, A. Kettrup, Fresen. J. Anal. Chem. 361 (1998) 124–128.
[12] P. Santhosh, K.M. Manesh, A. Gopalan, K.P. Lee, Anal. Chim. Acta 575 (2006) 32–38.
[13] Y. Shen, M. Trauble, G. Wittstock, Anal. Chem. 80 (2008) 750–759.
[14] J. Liu, C. Guo, C.M. Li, Y. Li, Q. Chi, X. Huang, L. Liao, T. Yu, Electrochem. Commun. 11 (2009) 202–205.
[15] Q. Rui, K. Komori, Y. Tian, H. Liu, Y. Luo, Y. Sakai, Anal. Chim. Acta 670 (2010) 57–62.
[16] S. Chen, R. Yuan, Y. Chai, L. Zhang, N. Wang, X. Li, Biosens. Bioelectron. 22 (2007) 1268–1274.
[17] C. Guo, F. Hua, C.M. Li, P.K. Shen, Biosens. Bioelectron. 24 (2008) 819–824.
[18] S. George, H.K. Lee, J. Phys. Chem. B 113 (2009) 15445–15454.
[19] B.X. Gu, C.X. Xu, G.P. Zhu, S.Q. Liu, L.Y. Chen, M.L. Wang, J.J. Zhu, J. Phys. Chem. B 113 (2009) 6553–6557.
[20] Z. Zhao, W. Lei, X. Zhang, B. Wang, H. Jiang, Sensors 10 (2010) 1216–1231.
[21] Z.M. Liu, Y. Yang, H. Wang, Y.L. Liu, G.L. Shen, R.Q. Yu, Sens. Actuators B: Chem. 106 (2005) 394–400.
[22] Y. Xiao, F. Patolsky, E. Katz, J.F. Hainfeld, I. Willner, Science 299 (2003) 1877–1881.
[23] W.J. Parak, T. Pellegrino, C.M. Micheel, D. Gerion, S.C. Williams, A.P. Alivisatos, Nano Lett. 3 (2003) 33–36.
[24] A. Gole, C. Dash, C. Soman, S.R. Sainkar, M. Rao, M. Sastry, Bioconjugate Chem. 12 (2001) 684–690.
[25] K.J. Huang, D.J. Niu, J.Y. Sun, X.L. Zhu, J.J. Zhu, Anal. Bioanal. Chem. 397 (2010) 3553–3561.
[26] S.J. Guo, S.J. Dong, Chem. Soc. Rev. 40 (2011) 2644–2672.
[27] H.B. Wang, T.T. Chen, S. Wu, X. Chu, R.Q. Yu, Biosens. Bioelectron. 34 (2012) 88–93.
[28] K.J. Huang, J. Li, Y.M. Liu, X.Y. Cao, S. Yu, M. Yu, Microchim. Acta 177 (2012) 419–426.
[29] M. Zhou, Y. Zhai, S. Dong, Anal. Chem. 81 (2009) 5603–5613.
[30] G.P. Kotchey, B.L. Allen, H. Vedala, N. Yanamala, A.A. Kapralov, Y.Y. Tyurina, J. Klein-Seetharaman, V.E. Kagan, A. Star, ACS Nano 5 (2011) 2098–2108.
[31] Z. Yin, S. Sun, T. Salim, S. Wu, X. Huang, Q. He, Y.M. Lam, H. Zhang, ACS Nano 4 (2010) 5263–5268.
[32] S. Ghosh, B.K. Sarker, A. Chunder, L. Zhai, S.I. Khondaker, Appl. Phys. Lett. 96 (2010) 163109–163111.
[33] R. Muszynski, B. Seger, P.V. Kamat, J. Phys. Chem. C 112 (2008) 5263–5266.
[34] Y.L. Yao, Y. Ding, L.S. Ye, X.H. Xia, Carbon 44 (2006) 61–66.
[35] K.J. Huang, Y.X. Miao, L. Wang, T. Gan, M. Yu, L.L. Wang, Process Biochem. 47 (2012) 1171–1177.
[36] K.J. Huang, J.Y. Sun, C.X. Jin, Q.S. Jing, T. Zhou, Thin Solid Films 519 (2011) 3925–3930.
[37] S. Wei, W. Dandan, G. Ruifang, J. Kui, Electrochem. Commun. 9 (2007) 1159–1164.
[38] S. Wang, T. Chen, Z. Zhang, X. Shen, Z. Lu, D. Pang, K. Wong, Langmuir 21 (2005) 9260–9266.
[39] S. Wang, T. Chen, Z. Zhang, D. Pang, K. Wong, Electrochem. Commun. 9 (2007) 1709–1714.
[40] C. Yu, X. Zhou, H. Gu, Electrochim. Acta 55 (2010) 8738–8743.
[41] M. Song, X. Feng, X. Lu, X. Wang, Electroanalysis 22 (2010) 668–672.
[42] L. Wang, Q. Ran, Y. Tian, J. Xu, Y. Xian, R. Peng, L. Jin, J. Colloid Interface Sci. 350 (2010) 544–550.
[43] C.X. Lei, S.Q. Hu, N. Gao, G.L. Shen, R.Q. Yu, Bioelectrochemistry 65 (2004) 33–39.
[44] J. Zhang, M. Oyama, Electrochim. Acta 50 (2004) 85–90.
[45] X. Han, W. Huang, J. Jia, S. Dong, E. Wang, Biosens. Bioelectron. 17 (2002) 741–746.
[46] Q. Wang, G. Lu, B. Yang, Sens. Actuators B: Chem. 99 (2004) 50–57.
[47] Y.D. Zhao, Y.H. Bi, W.D. Zhang, Q.M. Luo, Talanta 65 (2005) 489–494.
[48] A.K.M. Kafi, D.Y. Lee, S.H. Park, Y.S. Kwon, Microchem. J. 85 (2007) 308–313.
[49] D. Shan, S.X. Wang, H.G. Xue, S. Cosnier, Electrochem. Commun. 9 (2007) 529–534.